

# FastLGS: Speeding up Language Embedded Gaussians with Feature Grid Mapping

YUZHOU JI\*, East China Normal University, China  
 HE ZHU\*, East China Normal University, China  
 JUNSHU TANG, Shanghai Jiao Tong University, China  
 WUYI LIU, East China Normal University, China  
 ZHIZHONG ZHANG, East China Normal University, China  
 YUAN XIE, East China Normal University, China  
 XIN TAN†, East China Normal University, China

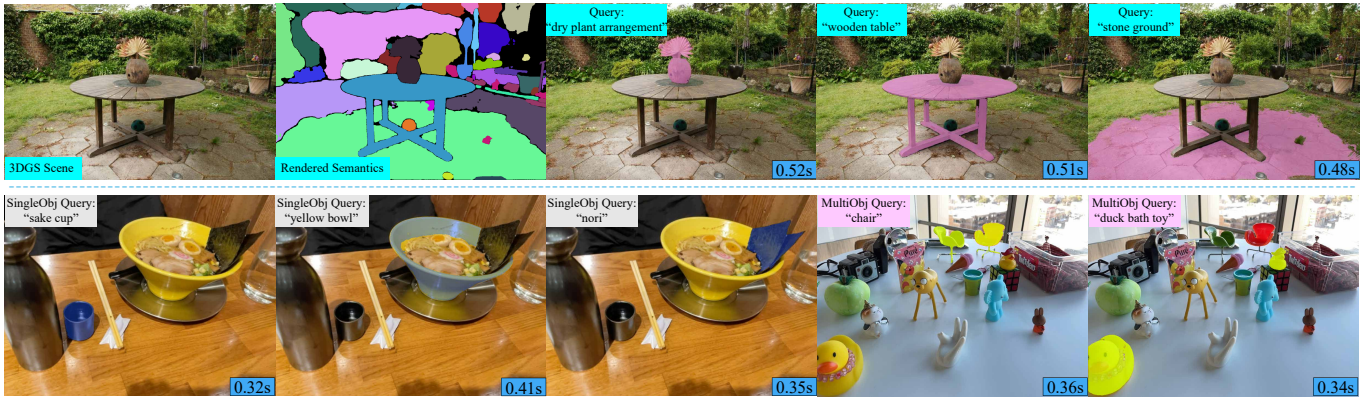


Fig. 1. Open-vocabulary query results from FastLGS in reconstructed scenes, which has the ability to generate high quality masks of single or multiple objects having the same semantics in novel views under interactive time consumption. The displayed query times are from rendering resolution 1297x840 (line 1) and 989x731 (line 2).

The semantically interactive radiance field has always been an appealing task for its potential to facilitate user-friendly and automated real-world 3D scene understanding applications. However, it is a challenging task to achieve high quality, efficiency and zero-shot ability at the same time with semantics in radiance fields. In this work, we present FastLGS, an approach that supports real-time open-vocabulary query within 3D Gaussian Splatting (3DGS) under high resolution. We propose the semantic feature grid to save multi-view CLIP features which are extracted based on Segment Anything Model (SAM) masks, and map the grids to low dimensional features for semantic field training through 3DGS. Once trained, we can restore pixel-aligned CLIP embeddings through feature grids from rendered features for open-vocabulary queries. Comparisons with other state-of-the-art methods prove that FastLGS can achieve the first place performance concerning both **speed** and **accuracy**, where FastLGS is  $98\times$  faster than LERF and  $4\times$  faster than LangSplat. Meanwhile, experiments show that FastLGS is adaptive and compatible with many downstream tasks, such as 3D segmentation and 3D object inpainting, which can be easily applied to other 3D manipulation systems. The project page is at <https://george-attano.github.io/FastLGS/>.

\*Equal contribution.

†Corresponding author.

Authors' addresses: Yuzhou Ji, East China Normal University, Shanghai, China; He Zhu, East China Normal University, Shanghai, China; Junshu Tang, Shanghai Jiao Tong University, Shanghai, China; Wuyi Liu, East China Normal University, Shanghai, China; Zhizhong Zhang, East China Normal University, Shanghai, China; Yuan Xie, East China Normal University, Shanghai, China; Xin Tan, East China Normal University, Shanghai, China, [xtan@cs.ecnu.edu.cn](mailto:xtan@cs.ecnu.edu.cn).

CCS Concepts: • **Computing methodologies** → *Reconstruction; Scene understanding; Object detection*.

Additional Key Words and Phrases: open-vocabulary detection, zero-shot learning, semantic 3D field

## 1 INTRODUCTION

With the potential in fields such as robotics and augmented reality, 3D scene understanding has always been a conspicuous topic in the research community. Given a set of posed images, the goal is to learn an effective and efficient 3D semantic representation along with scene reconstruction, which should naturally support a wide range of downstream tasks in scene manipulation. However, it remains a vital challenge to simultaneously achieve **accuracy**, **efficiency** and the grounding of **open-vocabulary** level semantics together.

Predominantly, existing methods usually only focus on the accuracy of differentiating objects, which normally assign points with labels or low-level features. For example, Semantic-NeRF [Zhi et al. 2021], N3F [Tschernetzki et al. 2022] and Panoptic Lifting [Siddiqui et al. 2023] successfully lift labels or noisy 2D features into 3D radiance fields, providing semantic segmentations in certain scenes. However, their labels and low-level features (e.g., DINO [Caron et al. 2021] features) are not sufficient for natural modality interactions since some methods require extra position information (e.g., N3F [Tschernetzki et al. 2022]) and others even do not provide any

interaction (e.g., Semantic-NeRF[Zhi et al. 2021] and Panoptic Lifting[Siddiqui et al. 2023]), and they also suffer from poor quality concerning in-the-wild scenes due to the lack of zero-shot ability. One possible solution for introducing zero-shot semantics with friendly interactions is to use pre-trained text-image models with high-level features. LERF [Kerr et al. 2023], as one of the state-of-the-art examples, enables pixel-aligned queries of the distilled 3D CLIP [Radford et al. 2021] embeddings, supporting long-tail open-vocabulary queries. Nevertheless, despite solving the problem of open-vocabulary interactions, LERF’s results are completely not object-centric (in particular, it has been difficult to selectively edit specific regions or objects[Kobayashi et al. 2022]) and can only extract fuzzy relevancy maps, which might degrade in novel views because its non-object-centric CLIP ground truth under interpolation is neither 3D consistent nor accurate. The above discussion shows the dilemma of balancing open-vocabulary ability and localizing accuracy when building a semantic field, not to mention these NeRF-based methods also suffer from the slow rendering speed.

To get out of such a predicament, one may naturally think of achieving object-centric along with CLIP embeddings, but this brings numerous problems. First, we need to achieve the extraction of objects across all views to ensure object level 3D-consistency, where the popular Segment Anything Model (SAM) [Kirillov et al. 2023] is strong enough to serve. However, to be a zero-shot method without any other model guidance in the whole process, the raw multi-granularity SAM masks can be confusing for the many-to-many masks mapping of even a single object. Recent LangSplat [Qin et al. 2024] trains an auto-encoder to handle this issue, but the reconstructed features are degraded and not sufficient for demanding query tasks. Meanwhile, directly building a high-level CLIP field is not only time-consuming but also inconsistent across views because different views of one object can provide close but distinct CLIP features. Moreover, the query strategy is also largely determined by the building of a semantic field. If we query by computing the CLIP relevancy of each pixel as in LERF, it is still not affordable. These are all key challenges for building the interactive 3D semantic field.

Accordingly, in this paper, we present the FastLGS, which speeds up to build accurate 3D open-vocabulary semantic fields within 3D Gaussian Splatting (3DGS) [Kerbl et al. 2023] via the feature grid mapping strategy. Given a set of posed images, we ensure object-centric by using a mask-based method as the basis. FastLGS first extracts all SAM masks and sent through the CLIP encoder to extract object-level image features. While directly training a CLIP feature field in high dimensionality could be time-consuming, we build a feature grid to map CLIP features to lower 3D space, but which inherently creates a many-to-one mapping problem. To tackle the problem of many-to-one mapping problem in 3D-consistent mapping, we propose a cross-view feature matching strategy to assign feature grids that represent scene objects with all sides of semantics. The low-dimensional mappings are attached to Gaussians to build a feature field. During the inference stage, pixel-aligned features will be rendered and we restore their semantics within feature grids to generate results upon open-vocabulary queries.

During experiments, we found FastLGS can generate competitive target masks compared with state-of-the-art 3D segmentation and semantic field methods, grounding much more accurate language

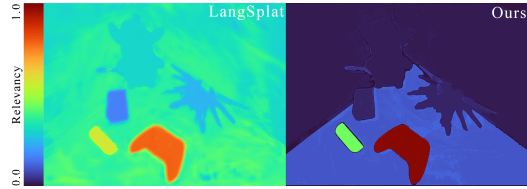


Fig. 2. Visualized relevancy (turbo) of query “Xbox wireless controller”. Our result is much more accurate in having higher relevancy within queried areas and lower relevancy among other regions compared with LangSplat.

embeddings than LangSplat (see Figure 2). Meanwhile, the FastLGS is fast and supports real-time interactions under high resolution ( $98\times$  faster than LERF and  $4\times$  faster than LangSplat, see Table 4), which can also be queried for single or multiple objects with similar queries in an adjustable way. Notably, FastLGS is adaptive and compatible with many downstream tasks that can be easily applied to systems like 3D segmentation and manipulation.

In summary, the principal contributions of this work include:

- To our best knowledge, this is the first work that can interactively generate scene target masks upon natural language queries under high resolution ( $1440\times 1080$ ) in real-time.
- We propose the grid mapping strategy with the zero-shot open-vocabulary prompted paradigm for building a 3D semantic field in 3DGS. As far as we know, our method is one of the **fastest** and **most accurate** methods in generating pixel-aligned semantic features in the 3D space.
- We provide an efficient 3D semantic basis and find it adaptive to easily integrate with several downstream tasks like 3D segmentation and 3D object inpainting.

## 2 RELATED WORKS

### 2.1 NeRF and 3D Gaussian Splatting (3DGS)

Neural Radiance Fields (NeRF) and 3D Gaussian Splatting (3DGS) have revolutionized 3D scene modeling and rendering. Introduced by [Mildenhall et al. 2021], NeRF synthesizes photorealistic scenes from sparse images by modeling volumetric density and color, further enhanced by innovations like mip-nerf [Barron et al. 2021] and TensorRF [Chen et al. 2022]. 3D Gaussian Splatting, detailed by [Kerbl et al. 2023] and expanded upon in work [Luiten et al. 2024] on dynamic 3D Gaussians, optimizes the rendering of point clouds with Gaussian kernels for real-time applications. These developments continue to advance the field, highlighting the dynamic growth and application breadth of these technologies. Additional contributions by [Tang et al. 2023b] and others [Fang et al. 2022] underscore the ongoing enhancements and versatility of 3DGS in handling increasingly complex rendering tasks. Noting the advantages of 3D Gaussian Splatting in rendering speed and quality, our paper chooses it as a representation for building semantic field.

### 2.2 2D and 3D Segmentation

The field of 2D image segmentation has undergone remarkable advancements since the introduction of Fully Convolutional Networks (FCN) [Long et al. 2015], which transformed traditional Convolutional Neural Networks (CNN) into architectures capable of pixel-wise predictions, revolutionizing segmentation tasks. This

innovation spurred expansive growth, with significant contributions like Mask R-CNN [He et al. 2017], which added a branch for object mask prediction to Faster R-CNN, and the adoption of Transformer architecture, notably through SEgmentation TRansformer (SETR) [Zheng et al. 2021], alongside studies [Cheng et al. 2022, 2021; Strudel et al. 2021; Xie et al. 2021]. These works demonstrated the Transformer’s potential in capturing complex dependencies for enhanced semantic segmentation. Recent innovations such as SAM [Kirillov et al. 2023] and SEEM [Zou et al. 2023] utilize various kinds of prompts for segmentation, inspired many mask based researches.

Advancements in 3D segmentation have paralleled those in 2D, with significant breakthroughs such as PointNet [Qi et al. 2017a] and PointNet++ [Qi et al. 2017b], which revolutionized the direct processing of point sets for classification and segmentation. These technologies enhanced the handling of 3D data by adapting and scaling to capture intricate local structures. Further innovations include Recurrent Slice Networks (RSNets) [Huang et al. 2018] for improved volumetric data segmentation, and Cylinder3D [Zhou et al. 2020], tailored for LiDAR semantic segmentation in driving scenes. Following developments in radiance fields have also refined the precision and applicability of 3D segmentation techniques [Cen et al. 2023b; Goel et al. 2023; Tang et al. 2023a], but open-vocabulary text guided 3D segmentation remains a challenge for the lack of compatible semantic scene construction.

### 2.3 Semantic 3D scene

Advancements in semantic integration have significantly enhanced 3D modeling, notably through NeRF and 3DGS. [Zhi et al. 2021] introduced semantic layers into NeRF, setting the stage for enriched scene understanding. This has been further developed in studies such as LERF [Kerr et al. 2023], ISRF [Goel et al. 2023], DFF [Yen-Chen et al. 2022], and N3F [Tschernezki et al. 2022], which integrate detailed semantic segmentation to refine 3D visualizations.

In parallel, enhancements in 3DGS have also advanced semantic capabilities. The foundational work [Kerbl et al. 2023] and further developments [Gu et al. 2024; Ye et al. 2023] have refined the application of 3DGS in semantic segmentation tasks. The SAGA framework [Cen et al. 2023a] demonstrates the integration of detailed 2D segmentation outcomes into 3D models, enhancing semantic accuracy. LangSplat [Qin et al. 2024] explores incorporating language processing into 3DGS, adding a new layer to semantic interpretations in 3D scene modeling. However, with inconsistent or fuzzy results in varying views and slow query speed, the quality of semantic fields built by these approaches still limits their further applications.

## 3 METHOD

### 3.1 Overview

As in Figure 3, the input images are initially put for extracting SAM masks and CLIP embeddings (Sec 3.2). This information is utilized together for the building of a semantic feature grid and low-dim feature mapping (Sec 3.3 and Sec 3.4). Then, the obtained pixel-aligned low-dim features are learned in parallel with scene reconstruction according to Sec 3.5 where we describe the training for embedded features through Gaussians. At the inference stage, the built semantic field can be interactively queried for high quality

masks in novel views using natural language based on restored embeddings. The query strategy is demonstrated in Sec 3.6.

### 3.2 Initialization

First, we initialize the original semantics. Given input images  $\{\mathbf{I}_t | t = 0, 1, \dots, T\}$ , for each image  $\mathbf{I}_i$ , we utilize SAM to obtain *whole* segmentation masks  $\{M_{i,j} | j = 0, 1, \dots, m_i\}$  with a regular grid of  $32 \times 32$  point prompts and compute respective CLIP features  $\{\mathbf{L}_{i,j} | j = 0, 1, \dots, m_i\}$ . Masks and CLIP embeddings will be used for building feature grids along with pixel-aligned low-dim feature maps. After initialization, no other pre-trained model will be required except for a CLIP text encoder at the inference stage.

### 3.3 Semantic Feature Grid

By practice, simply integrating CLIP feature with 3DGS can lead to infeasible demand of memory and limited efficiency of rendering as each Gaussian needs to record and update a parameter in hundreds of dimensions (Sec 4.3). On the other hand, the CLIP features of an object could show unexpected variance due to the view angles, redundant background and complex occlusion, posing a challenge to maintaining consistency and accuracy of semantics in 3D scenes. As language features of the same object from multiple views should share similar semantics, it could be compressed for lower training and query costs. However, current MLP-based compressed and reconstructed features cannot provide queries of higher quality as the former can be inconsistent and inaccurate like the raw features while the latter can be degraded which is not sufficient for demanding scenes (see relevancy maps in Figure 2 and Figure 6). Meanwhile, similar methods also can not acquire unseen features in a single view, restricting the possibility of querying objects with semantics captured in another view but invisible through the current angle.

To address these issues, we propose semantic feature grid, which stores the multi-view language features of each object in the scene and is mapped to a low dimensional feature. Specifically, our goal is to map  $\mathbf{L} \in \mathbb{R}^D$  to  $\mathbf{f} \in (0, 1)^d$  where language features  $\mathbf{L}$  of the same object share the same low-dim feature  $\mathbf{f}$ . Each feature  $\mathbf{f}$  is assigned to a grid with the size of  $\mathcal{K}^{-\frac{1}{d}}$ , where  $\mathcal{K}$  refers to the number of objects in a specific scene computed during cross view matching (Sec 3.4). The low dimensional features will be assigned pixel-wise according to corresponding masks and trained efficiently in 3DGS, while the grid can be used to restore accurate CLIP embeddings based on rendered low-dim features during inference. In practice, this strategy enables our method to achieve less consumption and faster speed (Table 4).

### 3.4 Cross View Grid Mapping

To achieve consistent features of objects across views, we sequentially match the denoised masks in adjacent image set  $\mathbf{I}$  and assign features. Considering the possible instability of CLIP features in multi-views mentioned in Sec 3.3, the matching process consists of both key points correspondence and feature similarity comparison.

**Key points correspondence** We prioritize the mask correspondence by key points obtained using the SIFT and the k-nearest neighbors (KNN) algorithm for accurate and robust matching. The SAM masks with more than  $\tau$  corresponding key point pairs will be assigned to the same low dimensional feature  $\mathbf{f}$  and considered as segmentation masks of an object from different viewpoints.

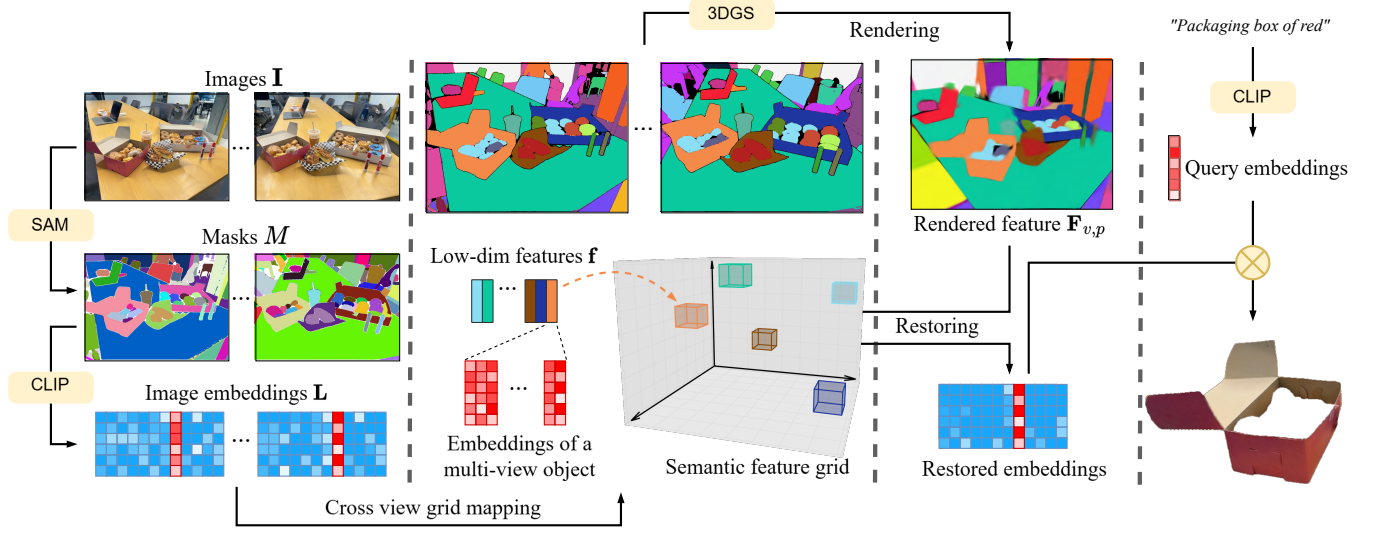


Fig. 3. FastLGS pipeline. Left: Initialization. Mid: Feature grid construction and embeddings restoring. Right: query using open-vocabulary prompts.

**Feature similarity comparison** As some segmentations with smooth pixel value have few key points, the matching process is employed according to similarity calculated by hybrid features of CLIP embedding  $\mathbf{L}$  and color distribution  $\mathbf{C}$ . For  $\mathbf{I}_i$  and  $\mathbf{I}_j$  with  $m_i$  and  $m_j$  mismatched masks, we calculate the similarity matrix  $\mathbf{SIM}_{m_i \times m_j}$  and choose the mask pairs with highest similarity. A threshold  $\theta$  is set that masks with similarity  $sim$  higher than  $\theta$  will have the same feature  $\mathbf{f}$  and the others will be assigned to a new low dimensional feature.

For two segmentation masks  $M_i, M_j$ , the similarity  $sim_{i,j}$  is calculated as follow:

$$\mathbf{sim}_{i,j} = \alpha \mathbf{sim}_{i,j}^{color} + (1 - \alpha) \mathbf{sim}_{i,j}^{CLIP}, \quad (1)$$

where  $\alpha$  is the weight of similarity of color distribution features  $\mathbf{C}$ .  $\mathbf{sim}_{i,j}^{CLIP}$  is calculated based on Bhattacharyya distance of  $\mathbf{C}$  while  $\mathbf{sim}_{i,j}^{color}$  is calculated by cosine similarity:

$$\mathbf{sim}_{i,j}^{CLIP} = \frac{\mathbf{L}_i \cdot \mathbf{L}_j}{\|\mathbf{L}_i\| \|\mathbf{L}_j\|}; \quad \mathbf{sim}_{i,j}^{color} = \sqrt{\mathbf{C}_i \mathbf{C}_j}. \quad (2)$$

Algorithm 1 displays our procedure of correspondence-based grid feature mapping. The consistency of objects across views is built and the amount  $\mathcal{K}$  is accessed during the matching process, which helps establish our semantic feature grids and low-dimensional feature mapping.

### 3.5 Training Features for Gaussians

We train a mapped low-dimensional feature  $\mathbf{f}_m$  for each gaussian  $g$  to build a feature field, which is adaptive for integration.

**Rendering Features** Given a camera pose  $v$ , we compute the feature  $\mathbf{F}_{v,p}$  of a pixel by blending a set of ordered Gaussians  $\mathcal{N}$  overlapping the pixel similar to the color computation of 3DGS:

$$\mathbf{F}_{v,p} = \sum_{i \in \mathcal{N}} \mathbf{f}_i a_i \prod_{j=1}^{i-1} (1 - a_j), \quad (3)$$

where  $a_i$  is given by evaluating a 2D Gaussian with covariance  $\Sigma$  multiplied with a learned per-Gaussian opacity.

**Optimization** The low-dim features follows 3DGS optimization pipeline and especially inherits the fast rasterization for efficient optimization and rendering. The loss function for features is  $\mathcal{L}_1$  combined with a D-SSIM term:

$$\mathcal{L}_f = (1 - \lambda) \mathcal{L}_1 + \lambda \mathcal{L}_{D-SSIM}, \quad (4)$$

where  $\lambda$  is also fixed to 0.2 in all cases.

### 3.6 Querying Features

Once trained, FastLGS can be interactively queried for different objects in the scene using open vocabulary text prompts. First, we query the pixel-aligned semantics  $\mathbf{F}_v$  by projecting the attached feature to view the plane using the rendering for features mentioned in Sec. 3.5, which can be used for all queries within camera pose  $v$ .

**Relevancy Score** When provided a prompt, we assign its language relevancy scores based on grid image features similar to LERF. We compute the cosine similarity between image embedding  $\phi_{img}$  and canonical phrase embeddings  $\phi_{canon}^i$ , then compute the pairwise softmax between image embedding and text prompt embedding  $\phi_{query}$ , so that the relevancy score is:

$$S_{relev} = \min_i \frac{\exp(\phi_{img} \cdot \phi_{query})}{\exp(\phi_{img} \cdot \phi_{canon}^i) + \exp(\phi_{img} \cdot \phi_{query})}. \quad (5)$$

For canonical phrases, we use “object”, “stuff” and “texture” for all queries.

**Target Mask** We go through feature grids to restore high-level image features and use them to compute relevancy with text embeddings. The grid with the highest relevancy score is deemed to be the target grid queried. Because each grid has multi-view image features of an object, we are even able to locate targets based on semantics invisible in the current query view (for example, locating a book named “computer vision” from the back of it). While

**ALGORITHM 1:** Grid Feature Mapping

---

**Input:** Image sequence  $\{\mathbf{I}_t | t = 0, 1, \dots, T\}$  with segmentation masks  $\{M_{i,j} | i = 0, 1, \dots, T; j = 0, 1, \dots, m_i\}$  CLIP features  $\{\mathbf{L}_{i,j} | i = 0, 1, \dots, T; j = 0, 1, \dots, m_i\}$  and color features  $\{\mathbf{C}_{i,j} | i = 0, 1, \dots, T; j = 0, 1, \dots, m_i\}$ , index of each mask  $M_{i,j}$ 's low dimensional feature  $Idx_{i,j}$ , parameters  $\alpha, \tau$  and  $\theta$

**Output:** low dimensional feature indices  $Idx$  of masks  $M$  and the number  $\mathcal{K}$  of objects in a scene

**for each image  $\mathbf{I}_i$  do**

**if  $i == 0$  then**

$\mathcal{K}, Idx_0 = \text{initialise}(\mathbf{I}_0, M_0, \mathbf{L}_0)$ ;

$\mathbf{I}^{prev} = \{\mathbf{I}_0\}; M^{prev} = \{M_{0,i} | i = 0, 1, \dots, m_0\}$ ;

**else**

$corrInfo = \text{correspondKp}(\mathbf{I}_i, \mathbf{I}^{prev}, M^{prev}, )$ ;

**for each mask  $M_{i,j}$  in image  $\mathbf{I}_i$  do**

$k, M_k^{prev}, numKp = \text{selMostCorrMask}(M_{i,j}, corrInfo)$ ;

**if  $numKp > \tau$  then**

$Idx_k^{prev} = \text{low-dim feature index of } M_k^{prev}$ ;

$Idx_{i,k} = Idx_k^{prev}$ ;

**else**

$sims_{i,j} = \text{computeSims}(M_{i,j}, M^{prev}, \mathbf{L}, \mathbf{C})$ ;

$k, M_k^{prev}, sim = \text{selMostSimMask}(M_{i,j}, M^{prev}, sims_{i,j})$ ;

**if  $sim > \theta$  then**

$Idx_k^{prev} = \text{low-dim feature index of } M_k^{prev}$ ;

$Idx_{i,j} = Idx_k^{prev}$ ;

**else**

$\mathcal{K} = \mathcal{K} + 1; Idx_k^{prev} = \mathcal{K}$ ;

**end**

**end**

$\mathbf{I}^{prev} = \text{union}(\mathbf{I}^{prev}, \{\mathbf{I}_i\})$ ;

$M^{prev} = \text{union}(M^{prev}, \{M_{i,j} | j = 0, 1, \dots, m_i\})$ ;

**end**

**end**

**end**

---

the rendered semantics have been smoothed, we locate their corresponding feature grids by calculating euclidean distance between grids and rendered features:  $Dis_{gf} = \sqrt{\sum_{i=0}^2 (\mathbf{F}_p^{v,i} - \mathbf{p}_i)^2}$  where  $\mathbf{p}$  denotes the grid's corresponding low-dim features. We compute pixel-wise  $Dis_{gf}$  based on target grid, and points with  $Dis_{gf}$  lower than threshold  $\tau_{ac}$  forms the target mask. By changing the number of grids used, we can adjustably query multiple targets (as Figure 1).

## 4 EXPERIMENTS

In this section, we first show the speed and quality of open-vocabulary object retrieval in comparison with other state-of-the-art methods through quantitative experiments in Sec 4.1, then we provide qualitative results of downstream tasks including 3D segmentation and object deletion in Sec 4.2. Ablation studies are in Sec 4.3 to demonstrate the rationality of feature grid based design.

**Datasets** For quantitative experiments, we train and evaluate the models on datasets including SPIn-NeRF [Mirzaei et al. 2023], LERF [Kerr et al. 2023] and 3D-OVS [Liu et al. 2023]. For experiments on

downstream applications we also used the MIP-360 dataset [Barron et al. 2022] (see example 4 of Figure 6).

**Implementation Details** We use the same OpenClip ViT-B/16 model as LERF and SAM ViT-H model as LangSplat. We train the features and scenes in 3DGS for 30,000 iterations. Activation threshold  $\tau_{ac}$ , correspondence threshold  $\tau$  and  $\theta$  are set to 5.0, 4 and 0.95. Weight  $\alpha$  is set to 0.3.  $\mathbf{f}$  is normalized to  $(0, 255)^3$ . Experiments show robustness of the proposed method to the aforementioned parameters. While the original time calculation of LangSplat puts aside feature rendering time and feature reconstructing time, here we compute the query time of the whole query process as LERF does. The tested LERF masks are regions with relevancy higher than 20% after normalization. The normalization for each query is from 50% (less relevant than canonical phrases) to the maximum relevancy, which is identical to the visualization strategy of LERF. All results are reported running on a single TITAN RTX GPU.

### 4.1 Comparison With Other State-of-the-art Methods

For quantitative experiments, we test different methods on the SPIn-NeRF dataset, the LERF dataset and 3D-OVS dataset. We show the quality of FastLGS-generated masks by comparing with other state-of-the-art 3D segmentation methods including the multi-view segmentation of SPIn-NeRF (MVSeg) [Mirzaei et al. 2023] and SA3D [Cen et al. 2023b], and compare the language retrieval ability with LERF [Kerr et al. 2023] and LangSplat [Qin et al. 2024].

**SPIn-NeRF dataset** We evaluate the IoU and pixel-wise accuracy of masks with provided ground truth ( $1008 \times 567$ ), and also show the time consumption for each query, which is omitted in MVSeg and SA3D because they do not support single view query. For LERF, LangSplat and FastLGS, we use the same text queries for the target segmentation objects to generate masks. Other methods all follow their original settings when tested on this dataset. We also provide the 2D segmentation results generated by SAM based on manual point prompts of original scene images for comparison. As shown in Table 1, FastLGS generates masks with competitive quality which have higher mIoU compared with other methods, and largely outperforms LERF and LangSplat in query speed.

**LERF dataset** The LERF dataset contains a number of in-the-wild scenes and is much more challenging, which strongly requires zero-shot abilities. We report localization accuracy for the 3D object localization task following LERF [Kerr et al. 2023] with ground truth annotations provided by LangSplat [Qin et al. 2024] (resolution around  $985 \times 725$ ). Results are shown in Table 2 and visual examples in Figure 4 (line 1&2), which further demonstrates FastLGS's advantages in natural language retrieval.

**3D-OVS dataset** We also compare with 2D-based open-vocabulary segmentation methods including ODISE [Xu et al. 2023] and OV-Seg [Liang et al. 2023] along with 3D-based methods including 3D-OVS [Liu et al. 2023], LERF [Kerr et al. 2023] and LangSplat [Qin et al. 2024]. Results are provided in Table 3, where our method can outperform both 2D and 3D methods. In Figure 4 (line 3) our method can also better support demanding custom query "keyboard and pocket tissues" which fails in LangSplat. Meanwhile, Figure 6 provides a visualization of pixel-aligned relevancy upon different queries, where our method has more accurate relevancy scores compared with LERF and LangSplat. Table 4 further shows the query time and

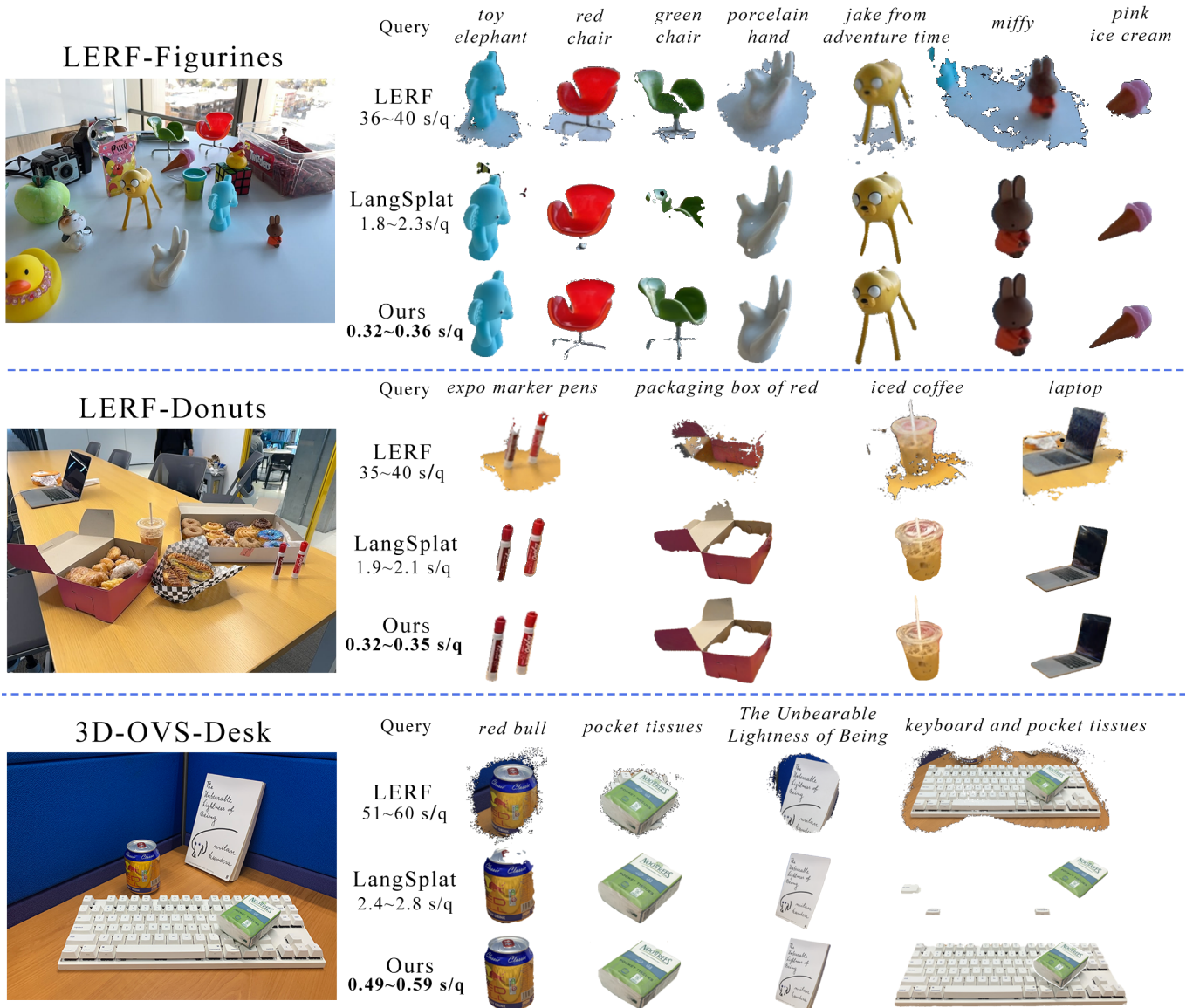


Fig. 4. Visual results of retrieved objects in different scenes.

model size where our method also outperforms LERF and LangSplat, proving its advantages in real-world applications.

#### 4.2 Downstream Applications

In this section, we test our method for the ability of applying to downstream 3D object manipulation tasks. Successful visual results are provided in Figure 6.

**Language Driven 3D Segmentation** We integrate FastLGS with Segment Any 3D Gaussians (SAGA) [Cen et al. 2023a] to achieve language driven 3D segmentation. SAGA attaches a low-dimensional 3D feature to each Gaussian in the trained 3DGS model to conduct mask-based segmentation. We attach our low-dim features to Gaussians in parallel with SAGA. The original SAGA requires manual

positional prompting for reference mask selection, but after integration we can directly use our masks as segmentation references and conduct 3D segmentation based on natural language. The whole query and segmentation process can be completed around only 1s.

**Language Driven Object Inpainting** We generate target masks of queried objects across views and use them as multi-view segmentation masks. We follow the multi-view segmentation based inpainting pipeline of SPIn-NeRF [Mirzaei et al. 2023] to conduct 3D object inpainting using the extracted multi-view segmentation masks. The masks are dilated by default with a 5x5 kernel for 5 iterations to ensure that all of the object is masked as in SPIn-NeRF.

Table 1. Quantitative Results on SPIn-NeRF dataset (LERF masks usually cover large surrounding areas and result in high mAcc and low mIoU).

Method	mIoU (%)	mAcc (%)	mTime (s)
SAM(2D)	95.7	96.1	0.05
MVSeg	89.5	97.8	-
SA3D	90.9	98.3	-
LERF	81.0	<b>99.5</b>	30.2
LangSplat	92.2	94.7	1.43
LEGaussians	89.3	97.8	1.04
OURS	<b>93.1</b>	95.2	<b>0.31</b>

Table 2. Quantitative Results of localization accuracy on LERF dataset.

Scene	LERF	LEGaussians	LangSplat	OURS
ramen	61.9	78.6	73.2	<b>84.2</b>
figurines	75.5	73.7	80.4	<b>91.4</b>
teatime	84.8	85.6	88.1	<b>95.0</b>
waldo_kitchen	70.2	90.1	95.5	<b>96.2</b>
Overall	73.1	82.0	84.3	<b>91.7</b>

Table 3. Quantitative Results of mIoU scores (%) on 3D-OVS dataset.

Method	<i>bed</i>	<i>bench</i>	<i>room</i>	<i>sofa</i>	<i>lawn</i>	Overall
ODISE	55.6	30.1	53.5	49.3	39.1	45.5
OV-Seg	79.8	88.9	71.4	66.1	81.2	77.5
3D-OVS	89.5	89.3	92.8	74.1	88.2	86.8
LERF	76.2	59.1	56.4	37.6	78.2	61.5
LangSplat	92.6	93.2	94.1	89.3	94.5	92.7
LEGaussians	45.7	47.4	44.7	48.2	49.7	47.14
OURS	<b>94.7</b>	<b>95.1</b>	<b>95.3</b>	<b>90.6</b>	<b>96.2</b>	<b>94.4</b>

Table 4. Comparison of performance and consumption (time computed on rendering resolution 1440x1080).

Scene “sofa”	LERF	LangSplat	OURS
mTime (s/q)	51.2	2.14	<b>0.52</b>
Model Size	1.28GB	565MB	<b>200MB</b>

Results show that consistent masks can be directly used for high-quality object inpainting through 3D inpainting methods.

According to the above experiments in Sec 4.1 and Sec 4.2, our method proves to be superior in grounding accurate semantics with interactive efficiency and more affordable consumption, further paving the way for many downstream 3D manipulation tasks in open-vocabulary interaction development.

### 4.3 Ablations

We conduct ablation to validate the necessity of our semantic feature grid for query and the improvements for the accuracy of our components in building cross-view grid mapping.

Table 5. Ablation on querying feature.

Component			Performance	
SAM	3D-GS	SFG	mIoU(%)	mTime(s)
✓			83.3	20.1
✓	✓		OOM	OOM
✓	✓	✓	95.1	0.98

Table 6. Ablation on the semantic feature grid.

Component			Performance	
CLIP	KP	CD	mIoU(%)	mAcc(%)
✓			75.2	83.2
✓	✓		87.5	91.8
✓	✓	✓	92.1	97.5

**Querying Feature** The performance is reported in Table 5, where SFG represents the semantic feature grid. Initially, we directly reconstruct the semantic field with NeRF using extracted CLIP features for SAM-based masks of images. When replacing NeRF with 3D Gaussian Splatting, the high dimensions of CLIP feature result in running out of memory. The issue is addressed by combining it with a semantic feature grid, which also brings improvements in accuracy and speed.

**Cross view** We report results in Table 6 and Figure 5, where KP represents key points and CD represents color distribution feature C. Key points correspondence and features similarity with the auxiliary of color distribution provide more guidance for maintaining consistency of objects across a series of continuous perspectives, which are dedicated to training low-dim features of high quality for Gaussians and effectively improving the performance.

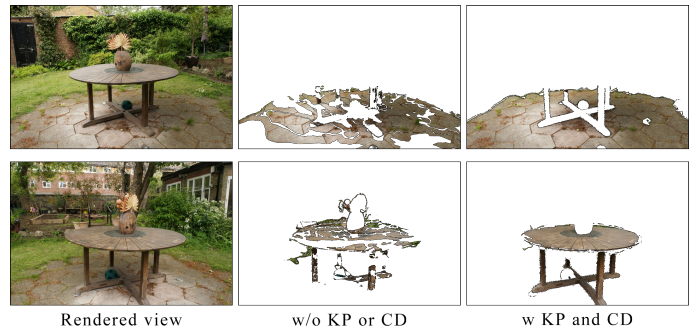
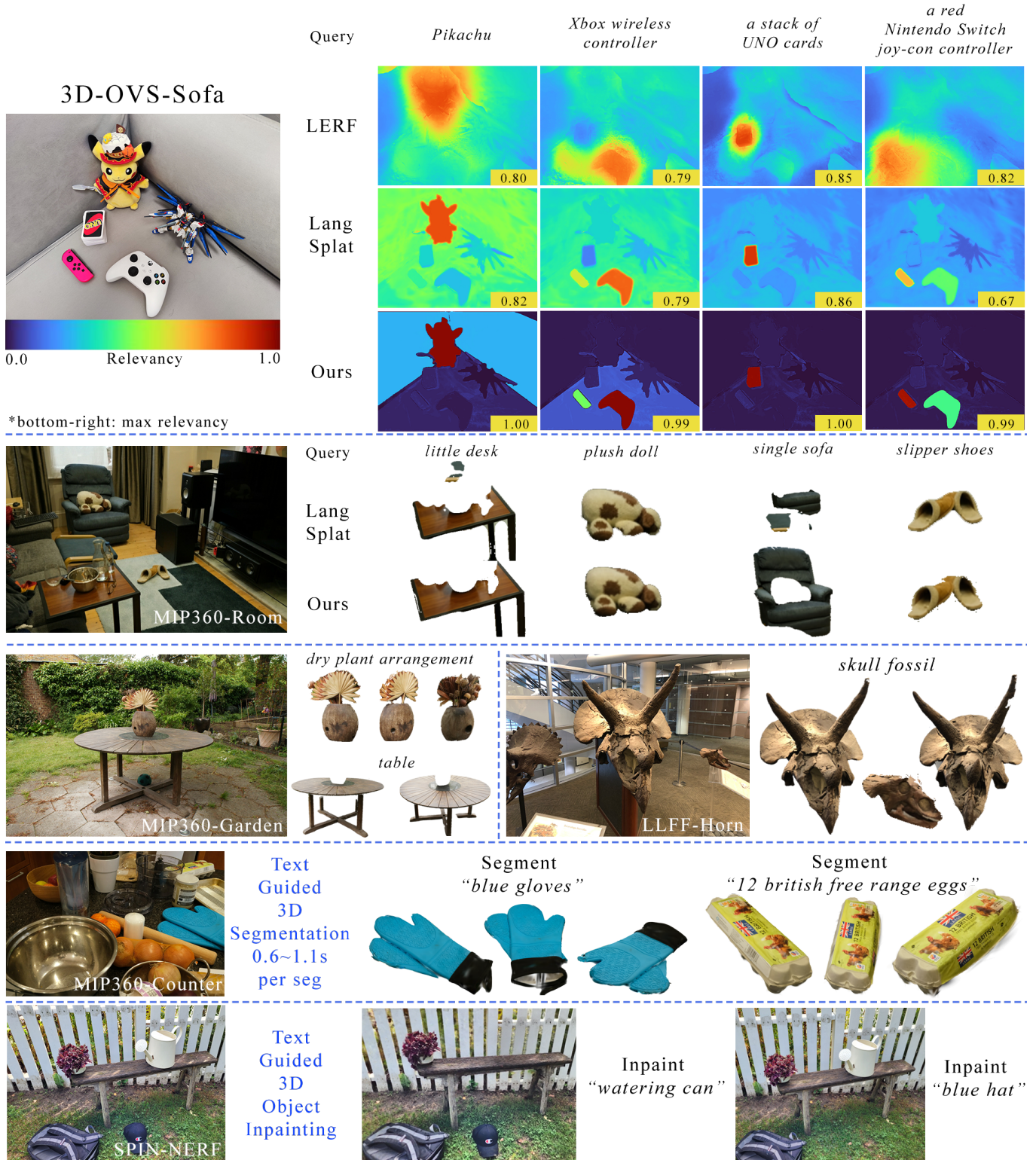


Fig. 5. Ablation on keypoint and color feature matching.

## 5 CONCLUSIONS AND FUTURE WORK

In this paper, we propose FastLGS, a method that speeds up to build accurate 3D open-vocabulary semantic fields within 3DGS. By mapping and restoring multi-view CLIP embeddings through feature grids instead of MLPs, FastLGS not only has interactive query speed, but also provides more accurate target masks and semantic relevancy along with lower consumption compared with state-of-the-art methods. Meanwhile, experiments show FastLGS’s ability to





be integrated with other downstream 3D manipulation tasks. While FastLGS now follows an object-centric paradigm, challenges occur in querying for parts of an object, such as “bicycle handlebars” or “chair leg”. We believe this could possibly be solved by building the feature grid in a multi-granularity way, where actual performance (time and space) along with cross-view consistency of both mask extraction and query results remain a problem, which requires further researches.

## REFERENCES

- Jonathan T. Barron, Ben Mildenhall, Matthew Tancik, Peter Hedman, Ricardo Martin-Brualla, and Pratul P. Srinivasan. 2021. Mip-NeRF: A Multiscale Representation for Anti-Aliasing Neural Radiance Fields. In *Proceedings of the IEEE/CVF International Conference on Computer Vision (ICCV)*. 5855–5864.
- Jonathan T Barron, Ben Mildenhall, Dor Verbin, Pratul P Srinivasan, and Peter Hedman. 2022. Mip-nerf 360: Unbounded anti-aliased neural radiance fields. In *Proceedings of the IEEE/CVF Conference on Computer Vision and Pattern Recognition (CVPR)*. 5470–5479.
- Mathilde Caron, Hugo Touvron, Ishan Misra, Hervé Jégou, Julien Mairal, Piotr Bojanowski, and Armand Joulin. 2021. Emerging properties in self-supervised vision transformers. In *Proceedings of the IEEE/CVF International Conference on Computer Vision (ICCV)*. 9650–9660.
- Jiazhong Cen, Jiemin Fang, Chen Yang, Lingxi Xie, Xiaopeng Zhang, Wei Shen, and Qi Tian. 2023a. Segment Any 3D Gaussians. *arXiv preprint arXiv:2312.00860* (2023).
- Jiazhong Cen, Zanwei Zhou, Jiemin Fang, Wei Shen, Lingxi Xie, Dongsheng Jiang, Xiaopeng Zhang, Qi Tian, et al. 2023b. Segment Anything in 3D with NeRFs. *Advances in Neural Information Processing Systems* 36 (2023), 25971–25990.
- Anpei Chen, Zexiang Xu, Andreas Geiger, Jingyi Yu, and Hao Su. 2022. Tensorf: Tensorf radiance fields. In *European Conference on Computer Vision (ECCV)*. Springer, 333–350.
- Bowen Cheng, Ishan Misra, Alexander G. Schwing, Alexander Kirillov, and Rohit Girdhar. 2022. Masked-Attention Mask Transformer for Universal Image Segmentation. In *Proceedings of the IEEE/CVF Conference on Computer Vision and Pattern Recognition (CVPR)*. 1290–1299.
- Bowen Cheng, Alex Schwing, and Alexander Kirillov. 2021. Per-Pixel Classification is Not All You Need for Semantic Segmentation. In *Advances in Neural Information Processing Systems*, M. Ranzato, A. Beygelzimer, Y. Dauphin, P.S. Liang, and J. Wortman Vaughan (Eds.), Vol. 34. Curran Associates, Inc., 17864–17875.
- Jiemin Fang, Taoran Yi, Xinggang Wang, Lingxi Xie, Xiaopeng Zhang, Wenyu Liu, Matthias Nießner, and Qi Tian. 2022. Fast Dynamic Radiance Fields with Time-Aware Neural Voxels. In *SIGGRAPH Asia 2022 Conference Papers*. Association for Computing Machinery, New York, NY, USA, Article 11, 9 pages.
- Rahul Goel, Dhawal Sirikonda, Saurabh Saini, and P. J. Narayanan. 2023. Interactive Segmentation of Radiance Fields. In *Proceedings of the IEEE/CVF Conference on Computer Vision and Pattern Recognition (CVPR)*. 4201–4211.
- Qiao Gu, Zhaoyang Lv, Duncan Frost, Simon Green, Julian Straub, and Chris Sweeney. 2024. EgoLifter: Open-world 3D Segmentation for Egocentric Perception. *arXiv:2403.18118* [cs.CV]
- Kaiming He, Georgia Gkioxari, Piotr Dollar, and Ross Girshick. 2017. Mask R-CNN. In *Proceedings of the IEEE International Conference on Computer Vision (ICCV)*.
- Qiangui Huang, Weiyue Wang, and Ulrich Neumann. 2018. Recurrent Slice Networks for 3D Segmentation of Point Clouds. In *Proceedings of the IEEE Conference on Computer Vision and Pattern Recognition (CVPR)*.
- Bernhard Kerbl, Georgios Kopanas, Thomas Leimkühler, and George Drettakis. 2023. 3D Gaussian Splatting for Real-Time Radiance Field Rendering. *ACM Transactions on Graphics* 42, 4 (July 2023).
- Justin Kerr, Chung Min Kim, Ken Goldberg, Angjoo Kanazawa, and Matthew Tancik. 2023. LERF: Language Embedded Radiance Fields. In *Proceedings of the IEEE/CVF International Conference on Computer Vision (ICCV)*. 19729–19739.
- Alexander Kirillov, Eric Mintun, Nikhila Ravi, Hanzi Mao, Chloe Rolland, Laura Gustafson, Tete Xiao, Spencer Whitehead, Alexander C. Berg, Wan-Yen Lo, Piotr Dollar, and Ross Girshick. 2023. Segment Anything. In *Proceedings of the IEEE/CVF International Conference on Computer Vision (ICCV)*. 4015–4026.
- Sosuke Kobayashi, Eiichi Matsumoto, and Vincent Sitzmann. 2022. Decomposing NeRF for Editing via Feature Field Distillation. In *Advances in Neural Information Processing Systems*, Vol. 35.
- Feng Liang, Bichen Wu, Xiaoliang Dai, Kunpeng Li, Yanan Zhao, Hang Zhang, Peizhao Zhang, Peter Vajda, and Diana Marculescu. 2023. Open-vocabulary semantic segmentation with mask-adapted clip. In *Proceedings of the IEEE/CVF Conference on Computer Vision and Pattern Recognition (CVPR)*. 7061–7070.
- Kunhao Liu, Fangneng Zhan, Jiahui Zhang, Muyu Xu, Yingchen Yu, Abdulmoteleb El Saddik, Christian Theobalt, Eric Xing, and Shijian Lu. 2023. Weakly Supervised 3D Open-vocabulary Segmentation. *arXiv preprint arXiv:2305.14093* (2023).
- Jonathan Long, Evan Shelhamer, and Trevor Darrell. 2015. Fully Convolutional Networks for Semantic Segmentation. In *Proceedings of the IEEE Conference on Computer Vision and Pattern Recognition (CVPR)*.
- Jonathon Luiten, Georgios Kopanas, Bastian Leibe, and Deva Ramanan. 2024. Dynamic 3D Gaussians: Tracking by Persistent Dynamic View Synthesis. In *International Conference on 3D Vision (3DV)*.
- Ben Mildenhall, Pratul P Srinivasan, Matthew Tancik, Jonathan T Barron, Ravi Ramamoorthi, and Ren Ng. 2021. Nerf: Representing scenes as neural radiance fields for view synthesis. *Commun. ACM* 65, 1 (2021), 99–106.
- Ashkan Mirzaei, Tristan Aumentado-Armstrong, Konstantinos G Derpanis, Jonathan Kelly, Marcus A Brubaker, Igor Gilitschenski, and Alex Levinshstein. 2023. SPIn-NeRF: Multiview segmentation and perceptual inpainting with neural radiance fields. In *Proceedings of the IEEE/CVF Conference on Computer Vision and Pattern Recognition (CVPR)*. 20669–20679.
- Charles R. Qi, Hao Su, Kaichun Mo, and Leonidas J. Guibas. 2017a. PointNet: Deep Learning on Point Sets for 3D Classification and Segmentation. In *Proceedings of the IEEE Conference on Computer Vision and Pattern Recognition (CVPR)*.
- Charles Ruizhongtai Qi, Li Yi, Hao Su, and Leonidas J Guibas. 2017b. PointNet++: Deep Hierarchical Feature Learning on Point Sets in a Metric Space. In *Advances in Neural Information Processing Systems*, Vol. 30.
- Minghan Qin, Wanhua Li, Jiawei Zhou, Haoqian Wang, and Hanspeter Pfister. 2024. LangSplat: 3D Language Gaussian Splatting. In *Proceedings of the IEEE Conference on Computer Vision and Pattern Recognition (CVPR)*.
- Alec Radford, Jong Wook Kim, Chris Hallacy, Aditya Ramesh, Gabriel Goh, Sandhini Agarwal, Girish Sastry, Amanda Askell, Pamela Mishkin, Jack Clark, et al. 2021. Learning transferable visual models from natural language supervision. In *International conference on machine learning*. PMLR, 8748–8763.
- Yawar Siddiqui, Lorenzo Porzi, Samuel Rota Buló, Norman Müller, Matthias Nießner, Angela Dai, and Peter Kotschieder. 2023. Panoptic Lifting for 3D Scene Understanding With Neural Fields. In *Proceedings of the IEEE/CVF Conference on Computer Vision and Pattern Recognition (CVPR)*. 9043–9052.
- Robin Strudel, Ricardo Garcia, Ivan Laptev, and Cordelia Schmid. 2021. Segmenter: Transformer for Semantic Segmentation. In *Proceedings of the IEEE/CVF International Conference on Computer Vision (ICCV)*. 7262–7272.
- Jiaxiang Tang, Jiawei Ren, Hang Zhou, Ziwei Liu, and Gang Zeng. 2023b. Dream-Gaussian: Generative Gaussian Splatting for Efficient 3D Content Creation. *arXiv:2309.16653* [cs.CV]
- Songlin Tang, Wenjie Pei, Xin Tao, Tanghui Jia, Guangming Lu, and Yu-Wing Tai. 2023a. Scene-Generalizable Interactive Segmentation of Radiance Fields. In *Proceedings of the 31st ACM International Conference on Multimedia*. 6744–6755.
- Vadim Tschernezki, Iro Laina, Diane Larlus, and Andrea Vedaldi. 2022. Neural Feature Fusion Fields: 3D Distillation of Self-Supervised 2D Image Representations. In *2022 International Conference on 3D Vision (3DV)*. 443–453.
- Enze Xie, Wenhai Wang, Zhiding Yu, Anima Anandkumar, Jose M. Alvarez, and Ping Luo. 2021. SegFormer: Simple and Efficient Design for Semantic Segmentation with Transformers. In *Advances in Neural Information Processing Systems*, M. Ranzato, A. Beygelzimer, Y. Dauphin, P.S. Liang, and J. Wortman Vaughan (Eds.), Vol. 34. Curran Associates, Inc., 12077–12090.
- Jiarui Xu, Sifei Liu, Arash Vahdat, Wonmin Byeon, Xiaolong Wang, and Shalini De Mello. 2023. Open-vocabulary panoptic segmentation with text-to-image diffusion models. In *Proceedings of the IEEE/CVF Conference on Computer Vision and Pattern Recognition (CVPR)*. 2955–2966.
- Mingqiao Ye, Martin Danelljan, Fisher Yu, and Lei Ke. 2023. Gaussian Grouping: Segment and Edit Anything in 3D Scenes. *arXiv:2312.00732* [cs.CV]
- Lin Yen-Chen, Pete Florence, Jonathan T. Barron, Tsung-Yi Lin, Alberto Rodriguez, and Phillip Isola. 2022. NeRF-Supervision: Learning Dense Object Descriptors from Neural Radiance Fields. In *2022 International Conference on Robotics and Automation (ICRA)*. 6496–6503.
- Sixiao Zheng, Jiachen Lu, Hengshuang Zhao, Xiatian Zhu, Zekun Luo, Yabiao Wang, Yanwei Fu, Jianfeng Feng, Tao Xiang, Philip H.S. Torr, and Li Zhang. 2021. Rethinking Semantic Segmentation From a Sequence-to-Sequence Perspective With Transformers. In *Proceedings of the IEEE/CVF Conference on Computer Vision and Pattern Recognition (CVPR)*. 6881–6890.
- Shuaifeng Zhi, Tristan Laidlow, Stefan Leutenegger, and Andrew J. Davison. 2021. In-Place Scene Labelling and Understanding With Implicit Scene Representation. In *Proceedings of the IEEE/CVF International Conference on Computer Vision (ICCV)*. 15838–15847.
- Hui Zhou, Xinge Zhu, Xiao Song, Yuexin Ma, Zhe Wang, Hongsheng Li, and Dahua Lin. 2020. Cylinder3D: An Effective 3D Framework for Driving-scene LiDAR Semantic Segmentation. *CoRR* abs/2008.01550 (2020).
- Xueyan Zou, Jianwei Yang, Hao Zhang, Feng Li, Linjie Li, Jianfeng Wang, Lijuan Wang, Jianfeng Gao, and Yong Jae Lee. 2023. Segment Everything Everywhere All at Once. In *Advances in Neural Information Processing Systems*, A. Oh, T. Neumann, A. Globerson, K. Saenko, M. Hardt, and S. Levine (Eds.), Vol. 36. Curran Associates, Inc., 19769–19782.